Electronic Supplementary Information

One-step electrodeposition of $Ni_xFe_{3-x}O_4$/Ni hybrid nanosheet arrays as highly active and robust electrocatalysts for oxygen evolution

Dongjie Li,[a] Suqin Liu,[ab] Guanying Ye,[a] Weiwei Zhu,[a] Kuangmin Zhao,[a] Meng Luo,[a] and Zhen He[ab]*

[a]College of Chemistry and Chemical Engineering, Central South University, Changsha, Hunan 410083, P. R. China.

[b]Hunan Provincial Key Laboratory of Chemical Power Sources, Central South University, Changsha, Hunan 410083, P. R. China

*Corresponding author.
E-mail address: zhenhe@csu.edu.cn

This file includes:

Fig. S1 to S13

Table S1 to S4

1. Potential-time (*E*-t) transient for the electrodeposition of $Ni_xFe_{3-x}O_4$ and $Ni_xFe_{3-x}O_4$/Ni NSAs

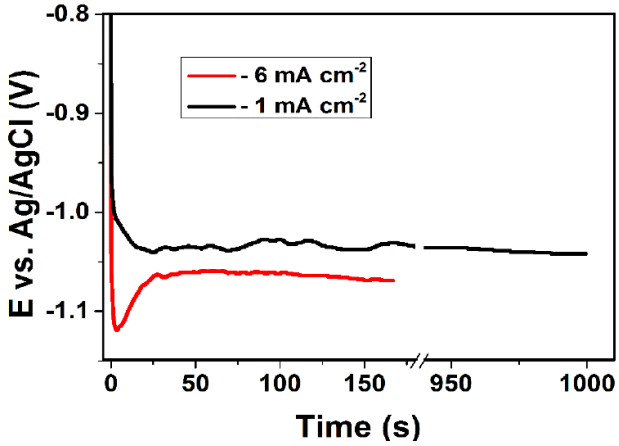

Fig. S1 *E*-t curves of electrodeposition of $Ni_xFe_{3-x}O_4$ and $Ni_xFe_{3-x}O_4$/Ni NSAs on the Au substrate at current densities of -1 and -6 mA cm^{-2} at 80 ℃ by passing 1 C cm^{-2} charge in the deposition solution containing 60 mM Ni^{2+}, 25 mM Fe^{3+}, 26.7 mM triethanolamine (TEA), 90 mM triethylenetetramine (TETRA), 0.1 M NH_4NO_3, and 2 M NaOH.

2. XRD study of the samples electrodeposited at different current densities

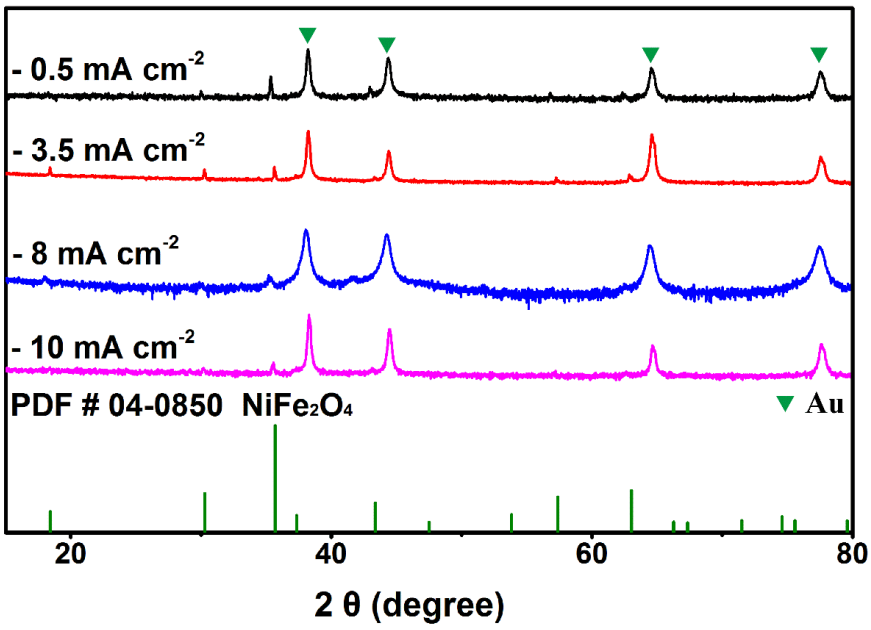

Fig. S2 XRD patterns of the samples electrodeposited at -0.5, -3.5, -8.0, and -10.0 mA cm^{-2}.

3. EDS, ICP, and XPS analysis on the Ni:Fe ratios in $Ni_xFe_{3-x}O_4$ and $Ni_xFe_{3-x}O_4$/Ni hybrid NSAs

Table S1 The atomic Ni:Fe ratios measured by EDS, ICP, and XPS in $Ni_xFe_{3-x}O_4$ and $Ni_xFe_{3-x}O_4$/Ni hybrid NSAs electrodeposited at -1 and -6 mA cm^{-2}.

Deposition current density (mA cm^{-2})	Ni:Fe ratio (by EDS)	Ni:Fe ratio (by ICP)	Ni:Fe ratio (by XPS)
-1	0.24	0.22	0.32
-6	0.42	0.46	0.44

4. SEM and EDS analysis of the $Ni_xFe_{3-x}O_4$/Ni electrodeposited at -10 mA cm^{-2}

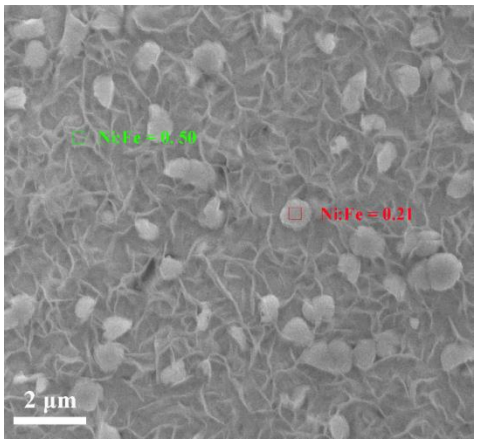

Fig. S3 SEM images of the $Ni_xFe_{3-x}O_4$/Ni electrodeposited at -10 mA cm^{-2}. The Ni:Fe ratios measured by EDS in the nanosheets and surface bulk structures are 0.5 and 0.21, respectively.

5. The influence of the additives on the OER activities of the $Ni_xFe_{3-x}O_4$/Ni hybrid NSAs

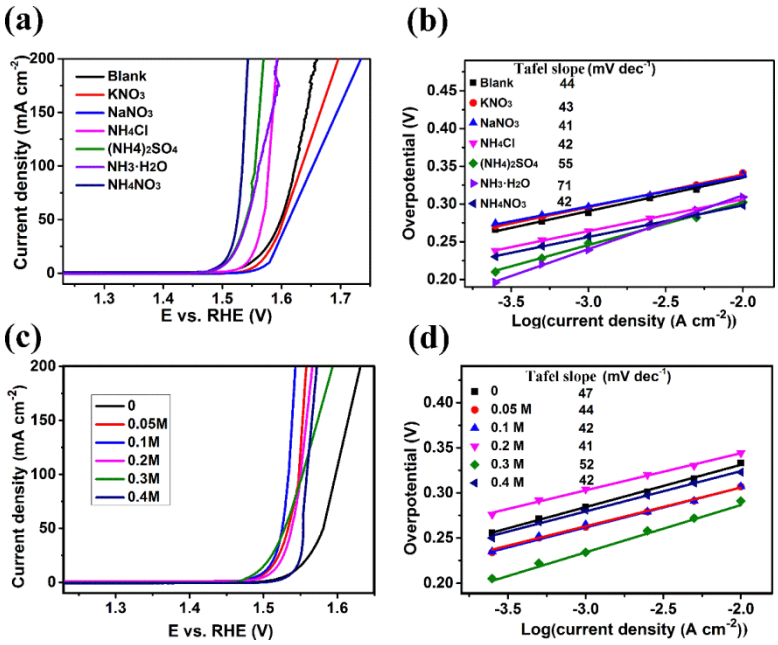

Fig. S4 (a) The LSV curves at a scan rate of 1 mV s^{-1} in 1.0 M KOH solution and (b) the corresponding Tafel plots on the $Ni_xFe_{3-x}O_4$/Ni samples electrodeposited with different additives at -6 mA cm^{-2}. (a) The LSV curves at a scan rate of 1 mV s^{-1} in 1.0 M KOH solution and (b) the corresponding Tafel plots on the $Ni_xFe_{3-x}O_4$/Ni samples electrodeposited with different concentrations of NH_4NO_3 (as the additive) at -6 mA cm^{-2}.

6. SEM images and EDS characterizations of the two parts of the $Ni_xFe_{3-x}O_4$/Ni hybrid NSA

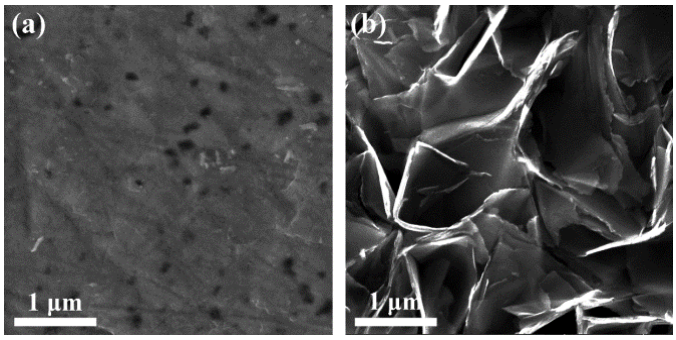

Fig. S5 SEM images of the (a) bottom dense layer and (b) upper nanosheet layer of the $Ni_xFe_{3-x}O_4$/Ni hybrid NSA electrodeposited at -6 mA cm^{-2} on Au. The upper nanosheet layer was peeled off from the bottom dense layer by using duct tape.

Table S2 The EDS measured overall Ni:Fe atomic ratio in the $Ni_xFe_{3-x}O_4$/Ni hybrid NSA electrodeposited at -6 mA cm^{-2} and the Ni:Fe atomic ratios in the upper and bottom layer of this $Ni_xFe_{3-x}O_4$/Ni hybrid NSA, respectively.

Sample	Ni:Fe ratio
$Ni_xFe_{3-x}O_4$/Ni (overall)	0.42
bottom dense layer	0.98
upper nanosheet layer	0.40

7. LSV study on the electrodeposition of $Ni_xFe_{3-x}O_4$/Ni hybrid NSAs

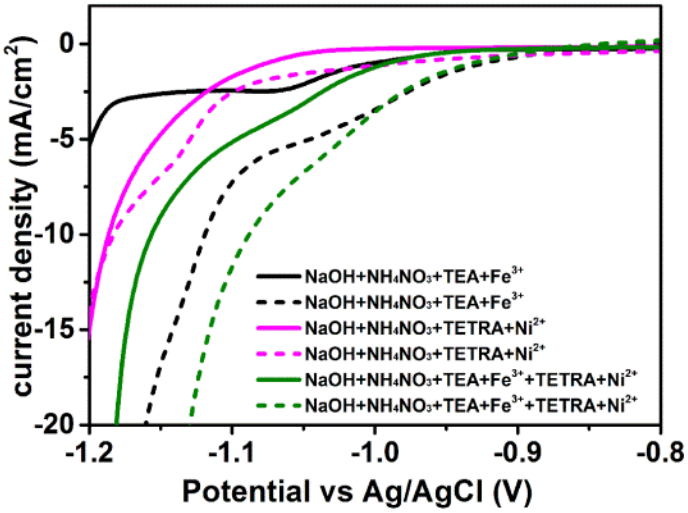

Fig. S6. LSV voltammograms on the bare Au substrate (solid curves) and the Au substrate covered with the dense layer of $Ni_xFe_{3-x}O_4$/Ni (after 40-s electrodeposition at -6 mA cm^{-2}) in different solutions.

8. Examples of the steady-state Tafel analysis of the electrodeposited $Ni_xFe_{3-x}O_4$ and $Ni_xFe_{3-x}O_4$/Ni NSAs

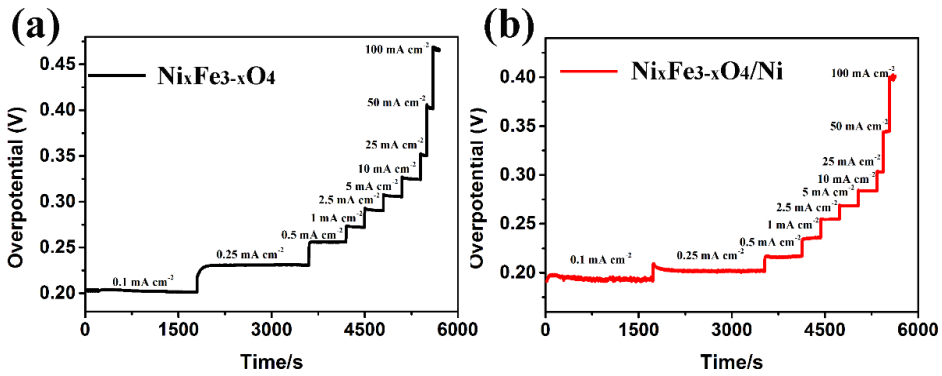

Fig. S7 The multi-current step measurements on the $Ni_xFe_{3-x}O_4$ and $Ni_xFe_{3-x}O_4$/Ni NSAs electrodeposited at -1.0 and -6.0 mA cm^{-2}. The applied current densities in the test are 0.1, 0.25, 0.5, 1, 2.5, 5, 10, 20, 50, 100 mA cm^{-2}. The time durations for the current steps (from low current density to high current density) are 1800, 1800, 600, 300, 300, 300, 300, 100, 100, and 100 s. The steady-state potential at each current step obtained on these plots is used for the steady-state Tafel plot in Fig. 5b.

9. Determination of the double-layer capacitance and electrochemically active surface area of the $Ni_xFe_{3-x}O_4$ and $Ni_xFe_{3-x}O_4$/Ni NSAs

The double-layer capacitance (C_{dl}) and electrochemically active surface area (ECSA) of the electrodeposited $Ni_xFe_{3-x}O_4$ and $Ni_xFe_{3-x}O_4$/Ni NSAs were estimated from the CV measurements. The CVs (Fig. S8a~g) of the $Ni_xFe_{3-x}O_4$ and $Ni_xFe_{3-x}O_4$/Ni NSA samples at different scan rates of 3, 4, 5, 6, 7, 8, 9, and 10 mV s^{-1} in 1 M KOH at room-temperature were performed in a potential window of OCP $\pm$20 mV. The C_{dl} is obtained from the slope of the linear fits to the current density (at open circuit potential (OCP)) vs scan rate plot ((Fig. S8h). The ECSA of each film is calculated according to the Eq. 1

$$\text{ECSA} = \frac{C_{dl}}{C_s} \times A \qquad (1)$$

where C_s (0.040 mF cm^{-2}) is the double-layer capacitance of $Ni_xFe_{3-x}O_4$ in 1 M KOH and A is

the geometric area of the fabricated $Ni_xFe_{3-x}O_4$ and $Ni_xFe_{3-x}O_4$/Ni NSA electrodes.[1]

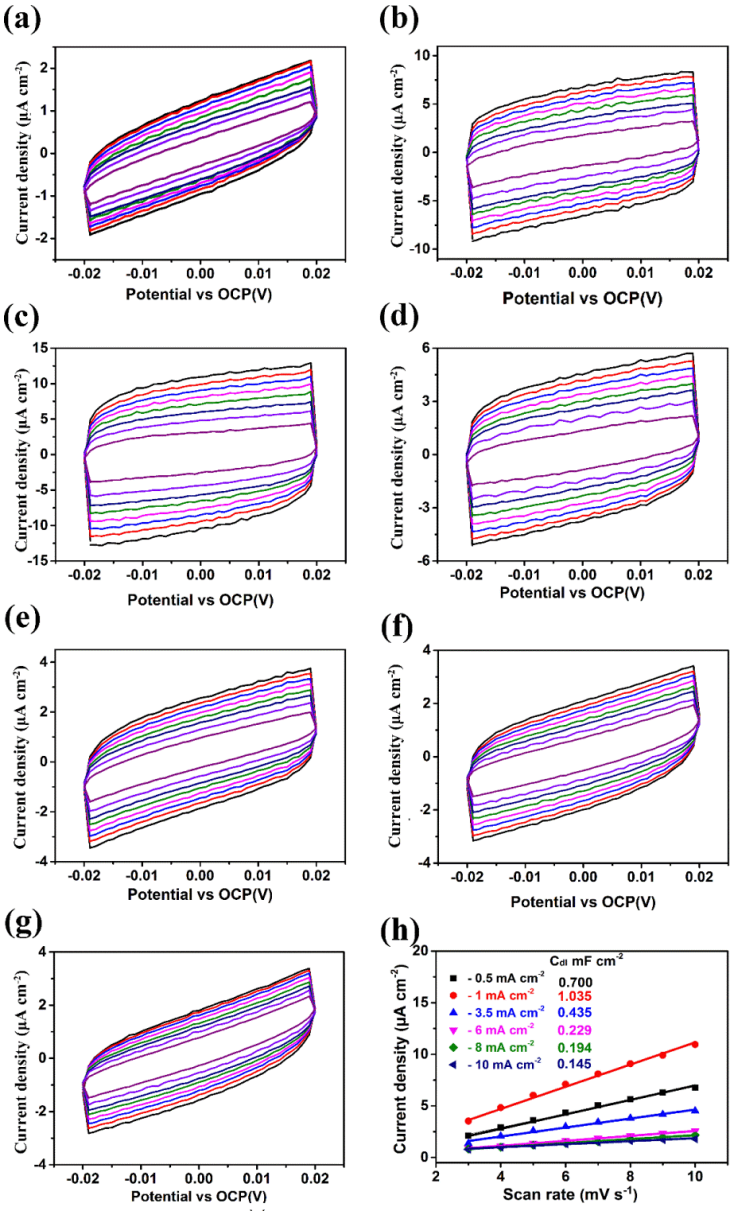

Fig. S8 CV curves at the scan rate of 3 (purple curve), 4 (violet curve), 5 (navy curve), 6 (olive curve), 7 (magenta curve), 8 (blue curve), 9 (red curve), and 10 (black curve) mV s^{-1} on (a) Au and the $Ni_xFe_{3-x}O_4$ and $Ni_xFe_{3-x}O_4$/Ni NSAs electrodeposited at (b) -0.5, (c) -1, (d) -3.5, (e) -6, (f) -8, and (g) -10 mA cm^{-2}. (h) Plots of the current density at 0 V vs. OCP as a function of scan rate.

10. Summary of the electrochemcial data of $Ni_xFe_{3-x}O_4$ and $Ni_xFe_{3-x}O_4$/Ni NSAs

Table S3 Summary of the main electrochemical data derived from the corresponding Measurements in Fig. 5.

Deposition current density ($mA\ cm^{-2}$)	Electrochemical data				
	η_{10} (mV)	η_{100} (mV)	Ts ($mV\ dec^{-1}$)	C_{dl} ($mF\ cm^{-2}$)	R_{ct} (Ω)
-0.5	346	440	57	0.700	45.48
-1	316	387	55	1.035	42.25
-3.5	302	364	37	0.435	30.14
-6	263	312	42	0.229	7.96
-8	280	326	51	0.194	10.99
-10	295	350	59	0.145	14.01
bare Au substrate	-	-	59	0.121	3099.93

η_{10} and η_{100}: overpotential obtained from the LSVs (in Fig. 5) at the current densities of 10 and 100 $mA\ cm^{-2}$.

Ts: Tafel slope.

C_{dl}: double-layer capacitance

R_{ct} : charge-transfer resistance

11. The stability test on $Ni_xFe_{3-x}O_4$/Ni NSA conducted at -10 $mA\ cm^{-2}$

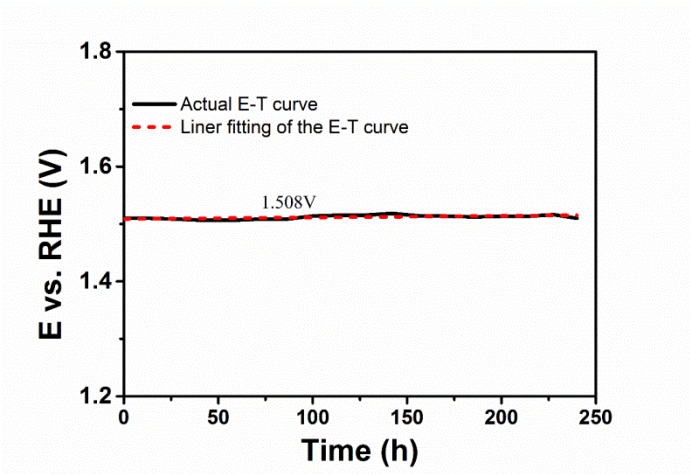

Fig. S9 Long-term stability test on the $Ni_xFe_{3-x}O_4$/Ni hybrid NSA (electrodeposited at -6 $mA\ cm^{-2}$) at 10 $mA\ cm^{-2}$ in 1 M KOH at room temperature for 10 days.

12. XPS study on the $Ni_xFe_{3-x}O_4$/Ni hybrid NSA before and after the stability test

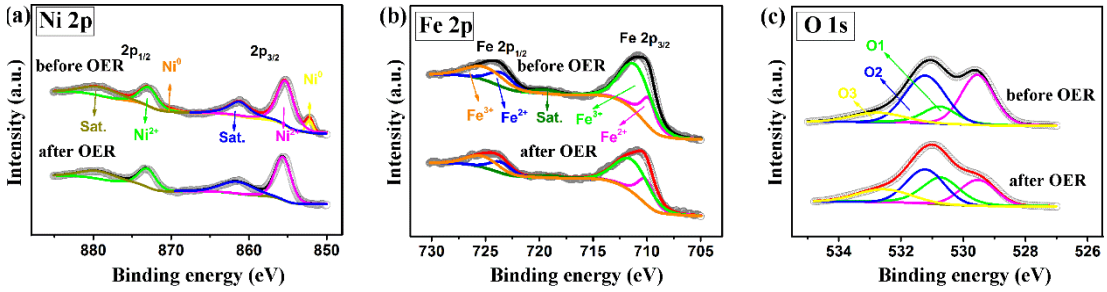

Fig. S10 (a) Ni 2p, (b) Fe 2p, and (c) O 1s XPS spectra of the $Ni_xFe_{3-x}O_4$/Ni hybrid NSA electrodeposited -6 mA cm^{-2} before and after the 240-h stability test at 10 mA cm^{-2} in 1 M KOH at room temperature.

13. Comparison of the OER activity of the $Ni_xFe_{3-x}O_4$/Ni hybrid NSAs electrodeposited on different planar substrates

The apparent catalytic performance of the prepared $Ni_xFe_{3-x}O_4$/Ni electrodes on different substrates (i.e., Au, GC, and SS) is similar (Fig. S11a). The LSV on SS (in the potential range of 1.43 to 1.53 V vs. RHE) slightly deviates from the LSV on the Au substrate, probably due to the slightly different electrochemically active surface area (which arises from the slightly different surface morphology) of the $Ni_xFe_{3-x}O_4$/Ni NSA deposited on SS compared to that on Au. This difference might also cause the slight variation of the Tafel slope on SS compared to that on Au (Fig. S11b). However, it is worth mentioning that the Tafel slopes on Au and SS are both consistent with the same OER mechanism involving one electrochemical preequilibrium step preceding a rate-limiting chemical step.[2]

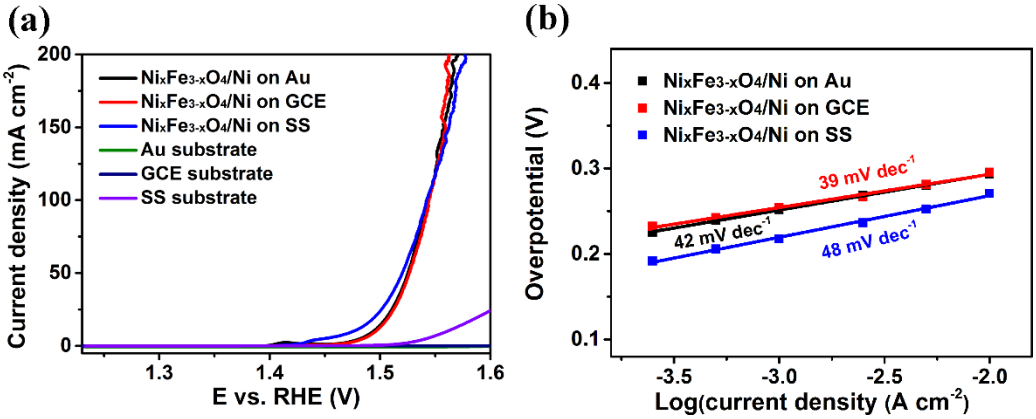

Fig. S11 (a) iR-corrected LSVs (at 1 mV s^{-1} in 1 M KOH) and (b) the corresponding steady-state Tafel plots of the $Ni_xFe_{3-x}O_4$/Ni hybrid NSAs electrodeposited at -6 mA cm^{-2} on the planar Au, GC, and SS substrates.

14. SEM and electrochemical characterizations of $Ni_xFe_{3-x}O_4$/Ni NSAs

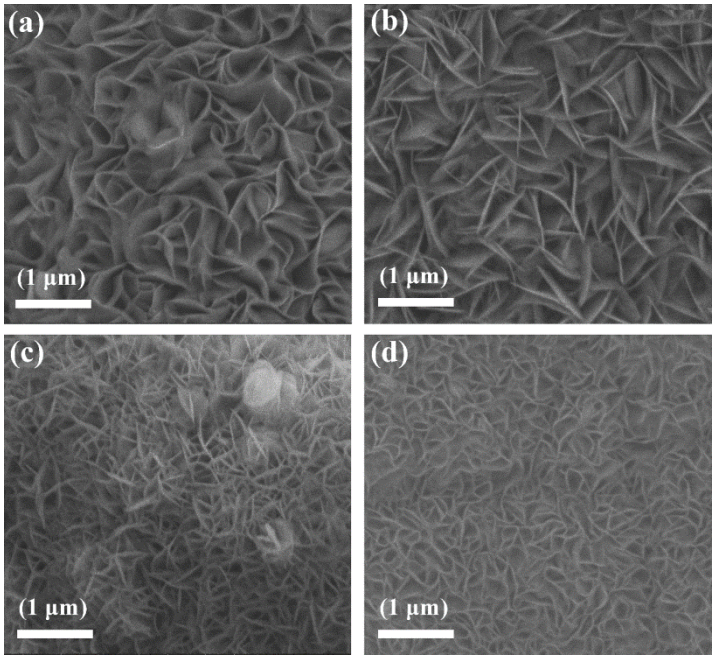

Fig. S12 SEM images of $Ni_xFe_{3-x}O_4$/Ni hybrid NSAs electrodeposited at (a) -1.06, (b) -1.07, and (c) -1.08 V for 200s on NF. (d) SEM image of the $Ni_xFe_{3-x}O_4$/Ni hybrid NSA deposited on NF at -1.07 V for 200s after the OER stability test at different current densities of 10, 50, 100, 150, 200, 250, 300, 350, 400, 450, 500 mA cm^{-2} for totally 220 h.

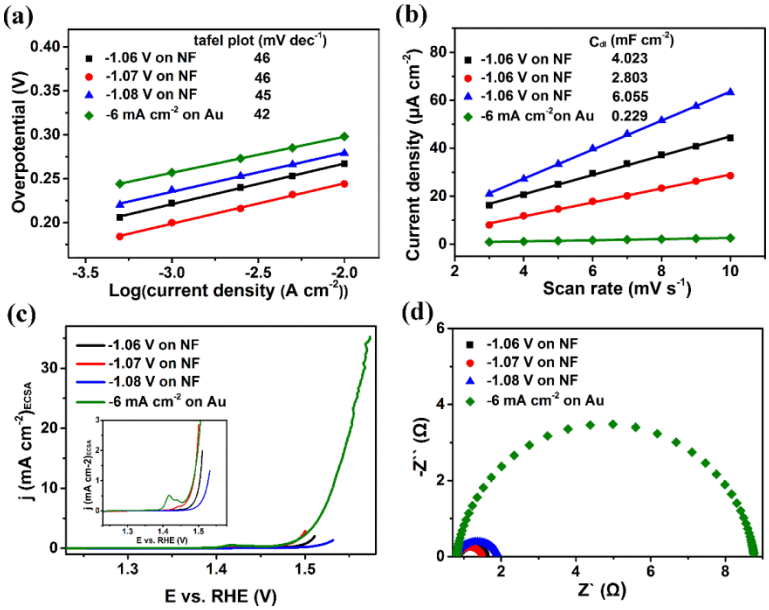

Fig. S13 Electrochemical properties of the $Ni_xFe_{3-x}O_4$/Ni hybrid NSAs electrodeposited at -1.06, -1.07, and -1.08 V on NF and -6 mA cm^{-2} on Au: (a) steady-state Tafel plots, (b) double-layer capacitance (C_{dl}), (c) ECSA-normalized LSV curves, and (d) Nyquist plots.

15. Comparison of the OER catalytic performance of the NiFe-based oxides

Table S4 Comparison between the OER performance of the $Ni_xFe_{3-x}O_4$/Ni hybrid NSA electrodeposited at -6 mA cm^{-2} on NF and the reported NiFe-based oxides OER catalysts in 1 M KOH aqueous solution.

Sample	η_{10}	Ts	Synthesis Methods	Time	Stability	Ref.
$NiFe_2O_4$ nano-rods/GCE ※	342	44	thermal decomposition	15 h	2 h @20mA cm^{-2}	3
FeNi/$NiFe_2O_4$@NC/GCE ※ ☆	316	60	metal-organic framework derivation	86 h	1.5 h @10 mA cm^{-2}	4
NiO/$NiFe_2O_4$/GCE ※ ☆	302	42	hydrothermal synthesis method and thermal decomposition	15 h	2 h @20 mA cm^{-2}	5
$NiFe_2O_4$/VACNT/NF ※ ☆	240	70	supercritical carbon dioxide ($SCeCO_2$)technique	8 h	8 h @10 mA cm^{-2}	6
2D $NiFe_2O_4$/GCE ※	460	193	hydrothermal synthesis method	10 h	N/A	7
1D $NiFe_2O_4$/NF ※ ☆	433	134	solution blow spinning	40 h	5.5 h @10 mA cm^{-2}	8
$Ni_{32}Fe$ oxides/NF ※	291	58	hard templating method	16 h	50 h @10 mA cm^{-2}	9
$NiFe_2O_4$/NF ※	343	185	eletrodeposition and annealing	2.5 h	N/A	10
Ni-Fe-O/GCE※	244	39	alloying/dealloying	3.5 h	60 h	11

					@10 mA cm^{-2}	
$Ni_xFe_{3-x}O_4$ /Ni/GCE ※ ☆	225	44	solvothermal	24 h	10 h @10 mA cm^{-2}	12
$NiFeO_x$@CuO NWs/Cu ※	300	40	electrodeposition	3.5 h	15 h @10 mA cm^{-2}	13
$NiFe_2O_4$ quantum dots /GCE ※	262	37	template method	78 h	100 h @10 mA cm^{-2}	14
$Ni_xFe_{3-x}O_4$/Ni/Au	**263**	**42**	**electrodeposition**	**167 s**	**240 h @10 mA cm^{-2}**	**this work**
$Ni_xFe_{3-x}O_4$/Ni/NF	**212**	**46**	**electrodeposition**	**200 s**	**250 h @10~500 mA cm^{-2}**	**this work**

※: Synthesis involves high temperature (>100 ℃) processes.

☆: Synthesis uses organic solvents (instead of DI water).

η_{10}: overpotential at a current density of 10 mA cm^{-2} during OER.

Ts: Tafel slope (mV dec^{-1}).

Time: the time of the synthesis.

References

1. C. C. L. McCrory, S. Jung, I. M. Ferrer, S. Chatman, J. C. Peters and T. F. Jaramillo, *J. Am. Chem. Soc.*, 2014, **137**, 4347.
2 J. B. Gerken, J. G. McAlpin, J. Y. C. Chen, M. L. Rigsby, W. H. Casey, R. D. Britt, S. S. Stahl, *J. Am Chem. Soc.* 2011, **133**, 14431.
3. G. Liu, K. Wang, X. Gao, D. He and J. Li, *Electrochim. Acta*, 2016, **211**, 871-878.
4. Y. Ma, X. Dai, M. Liu, J. Yong, H. Qiao, A. Jin, Z. Li, X. Huang, H. Wang and X. Zhang, *ACS Appl. Mater. Interfaces*, 2016, **8**, 34396.
5. G. Liu, X. Gao, K. Wang, D. He and J. Li, *Int. J. Hydrogen Energ.*, 2016, **41**, 17976-17986.
6. Y. Xu, Y. Yan, T. He, K. Zhan, J. Yang, B. Zhao, K. Qi and B. Y. Xia, *Carbon*, 2019, **145**, 201-208.
7. C. Mahala, M. D. Sharma and M. Basu, *Electrochim. Acta*, 2018, **273**, 462-473.
8. V. D. Silva, L. S. Ferreira, T. A. Simoes, E. S. Medeiros and D. A. Macedo, *J. Colloid Interf. Sci.*, 2019, **540**, 59-65.
9. M. Yu, G. Moon, E. Bill and H. Tüysüz, *ACS Appl. Energy Mater.*, 2019, **2**, 1199-1209.
10. J. Liu, D. Zhu, T. Ling, A. Vasileff and S.-Z. Qiao, *Nano Energy*, 2017, **40**, 264-273.
11. C. Dong, T. Kou, G. Hui, Z. Peng and Z. Zhang, *Adv. Energy Mater.*, 2018, **8**, 1701347
12. J. Huang, J. Han, R. Wang, Y. Zhang, X. Wang, X. Zhang, Z. Zhang, Y. Zhang, B. Song and S. Jin, *ACS Energy Lett.*, 2018, **3**, 1698-1707.
13. S. Czioska, J. Wang, S. Zuo, X. Teng and Z. Chen, *ChemCatChem*, 2018, **10**, 1005-1011.
14. H. Yang, Y. Liu, S. Luo, Z. Zhao, X. Wang, Y. Luo, Z. Wang, J. Jin and J. Ma, *ACS Catal.*, 2017, **7**, 5557-5567.